International Journal of Pavement Engineering

ISSN: (Print) (Online) Journal homepage: https://www.tandfonline.com/loi/gpav20

Potential contribution of steel slag fillers to asphalt mastic in terms of microwave heating efficiency, electromagnetic mechanisms and fatigue durability

Riran Wang, Tianyu Sha, Yuchao Xiong, Yingchun Cai, Jinchao Yue & Haopeng Wang

To cite this article: Riran Wang, Tianyu Sha, Yuchao Xiong, Yingchun Cai, Jinchao Yue & Haopeng Wang (2023) Potential contribution of steel slag fillers to asphalt mastic in terms of microwave heating efficiency, electromagnetic mechanisms and fatigue durability, International Journal of Pavement Engineering, 24:1, 2240471, DOI: 10.1080/10298436.2023.2240471

To link to this article: https://doi.org/10.1080/10298436.2023.2240471

Published online: 01 Aug 2023.

INTERNATIONAL JOURNAL OF PAVEMENT ENGINEERING
2023, VOL. 24, NO. 1, 2240471
https://doi.org/10.1080/10298436.2023.2240471

Potential contribution of steel slag fillers to asphalt mastic in terms of microwave heating efficiency, electromagnetic mechanisms and fatigue durability

Riran Wang[a], Tianyu Sha[a], Yuchao Xiong[a], Yingchun Cai[a], Jinchao Yue[a] and Haopeng Wang [b]

[a]Yellow River Laboratory, Zhengzhou University, Zhengzhou, Henan, People's Republic of China; [b]Nottingham Transportation Engineering Centre, Faculty of Engineering, University of Nottingham, Nottingham, United Kingdom

ABSTRACT

This paper investigates the potential contribution mechanisms of steel slag fillers in asphalt mastic, covering asphalt-filler interaction mechanisms, microwave heating efficiency, electromagnetic absorption mechanisms, and fatigue durability. The physico-chemical microscopic mechanisms of the steel slag filler, the limestone filler and the interactions between the fillers and the styrene-butadiene-styrene (SBS)-modified binders were characterized. The microwave-heating efficiency of steel slag-based asphalt mastic (SBS-SS) and limestone-based asphalt mastic (SBS-LS) was quantified. The dielectric behaviour of the fillers and the corresponding mastic was further characterized to reveal the electromagnetic mechanisms associated with the microwave heating technology. The stiffness evolution and the fatigue durability of SBS-based bitumen under the effectiveness of steel slag and limestone fillers were assessed by the viscoelastic continuum damage theory model and dissipative energy approaches. The steel slag fillers exhibited a greater potential to promote microwave heat efficiency than the natural stone fillers due to higher ferric oxide compositions. SBS-SS mastics have an overall greater dielectric constant and loss factor than those of SBS-LS mastics, resulting in superior electric field energy storage and conversion capabilities. The addition of steel slag fillers magnifies the load sensitivity of the bitumen and weakens the fatigue impedance and fatigue life of asphalt mastic composites.

ARTICLE HISTORY
Received 16 September 2022
Accepted 19 July 2023

KEYWORDS
Steel slag; asphalt mastic; microwave heating efficiency; electromagnetic mechanism; fatigue durability

1. Introduction

Steel slag, as a representative of industrial solid waste, will undoubtedly alleviate the problem of non-renewable stone consumption in pavement construction, thus reducing resource dependency and low carbon emissions in the construction process (Nadiatul Adilah *et al.* 2020). The field of research and development of new materials for pavement engineering is equally concerned with the recycling of steel slag materials. Researchers from around the world have given their conclusions and opinions on how a steelmaking slag with physical properties very close to or even better than natural stone can affect multi-layer asphalt pavement structures. Both basic oxygen furnace (BOF) steel slag (Chen *et al.* 2020, Pathak *et al.* 2020) and electric arc furnace (EAF) steel slag (Masoudi *et al.* 2017, Skaf *et al.* 2017, Ziaee and Behnia 2020) have been applied in asphalt mixtures as alternatives to coarse aggregate components. The aforementioned researchers have attempted to weather the steel slag coarse aggregates to provide the necessary volumetric stability to enable the steel slag based asphalt mixtures to meet the water stability requirements and to increase the application in drainage type pavements (Hainin *et al.* 2015). The conclusions drawn by Anastasiou *et al.* (2015) and Poulikalos *et al.* (2017) demonstrated that concrete pavements with high alternative content, such as steel slag waste, contribute more CO_2 emissions compared to natural stone concrete, which in turn enhances the environmental friendliness and sustainability of pavement construction. There is also research on the use of steel slag material as a cement-stabilised base course (Hainin *et al.* 2014, Barišić *et al.* 2014) or as an alternative to fully graded aggregates with various grain sizes in concretes (Hasita *et al.* 2020, Manso *et al.* 2006, Sosa *et al.* 2022). Yang et al. prepared artificial steel slag aggregates for better application in concrete by accelerating the carbonation behaviour of steel slag using an ethylenediamine tetra-acetic acid catalyst (Yang *et al.* 2021). Pasetto *et al.* (2017) have attempted to combine the warm mix technique with the utilisation of EAF-based steel slag instead of fillers and aggregates, and evaluated the mechanical properties of bitumen, mastic and mixes. A fine aggregate matrix (FAM) phase with steel slag filler by-products was found to exhibit better stiffness characteristics and fracture resistance by Fonseca *et al.* (2019). Chen et al. (2022b) have attempted to address the concern about the homogeneity of steel slag-based aggregates in asphalt mixtures by using industrially produced steel slag powders instead of natural stone fillers. An extensive review of the literature indicates that there is almost unanimous agreement that steel slag can be used to replace filler, fine or coarse aggregates in asphalt mixes and that the mechanical properties will meet all aspects of road performance requirements. As the demand for functional designs of asphalt-based pavement materials (self-sensing, self-cleaning, self-heating, self-healing, etc.) develops, the

CONTACT Haopeng Wang haopeng.wang@nottingham.ac.uk

focus on the material attributes of the steel slag itself and the underlying development in a particular performance area is more than ever expected.

Research into ways of extending the life of asphalt pavements is an attempt to address the current engineering problems of limited service life and frequent maintenance of pavements. Asphalt pavements in service are subject to long-term damage behaviour in the form of large scale micro-cracking due to traffic loads, climatic conditions, etc. Rapid pavement maintenance can help to slow down or even prevent major structural damage (e.g. reflective cracking). Rapid rehabilitation technology is highly desirable because on the one hand it enables rapid in-situ repair without disrupting traffic, and on the other hand it allows the reuse of old pavement concrete materials and reduces concrete consumption. As Agzenai *et al.* (2015) have outlined several innovative methods of pavement rehabilitation with great potential, namely microwave heating, induction heating, micro-encapsulation and ionomer utilisation. Among these, the microwave heating recovery approach requires the use of pavement materials with certain microwave absorption properties, these materials can be semiconductor, ferromagnetic material, metal oxides, dielectric material, metals (in powder or granular form) and mixtures as mentioned by Agzenai et al. in his review paper. Microwave-absorbing materials such as carbon-based materials (Wu and Tahri 2019, Lu *et al.* 2021, Li *et al.* 2018), magnetic iron oxides (Zhang *et al.* 2010, Guan *et al.* 2019), metallic fibres (García *et al.* 2009, Norambuena-Contreras and García 2016, Gallego *et al.* 2013, Wang *et al.* 2020a), Silicon carbide sand (Liu *et al.* 2021, Liu *et al.* 2020) and the industrial by-products mentioned in this study, steel slag, can contribute to the strong electromagnetic properties of asphalt mixtures. Steel slag is one of these, and according to current reports there are some preliminary studies using its microwave absorbing properties to heal or repair asphalt concrete. Pre-cracked three-point bending test and microwave heating repair test performed by Phan *et al.* (2018) demonstrated the applicability of steel slag in hot mix asphalt for the self-healing purpose under microwave irradiation. Cyclic crack-healing tests conducted by Lou *et al.* (2020) have proved that hot braised steel slag replacing 60% of the volume of coarse aggregate asphalt concrete has a strong potential for microwave heating and healing. As proposed by Gallego et al., the combined use of heating technology and an innovative re-compaction technique effectively facilitates the microwave heating and repair of EAF steel slag-based asphalt mortars (Gallego *et al.* 2021). In the previous work by us, the basic oxygen furnace (BOF) steel slag based fine aggregate matrix behaves better in microwave irradiation response and fatigue-healing performance than fine limestone-based asphalt mortar with experimental work carried out using a 2.45 GHz power microwave oven and rheological instrumentation platform (Wang *et al.* 2022). Furthermore, there are also studies focusing on snow and ice removal technology for steel slag-based asphalt concrete on snow-melting pavement related to electrical-thermal conductivity (Jiao *et al.* 2020a, Jiao *et al.* 2020b) and microwave heating technology (Gao *et al.* 2017). In addition, several innovative recent studies have investigated the temperature distribution (Chen *et al.* 2022a), self-healing properties of asphalt mixtures with steel slag aggregates under microwave heating technology (Liu *et al.* 2022).

The above study indicates that steel slag will undoubtedly enhance the microwave absorption potential of asphalt concrete, enhancing the repair potential and functionality such as de-icing technology. Yet as conventional asphalt concrete is not microwave inductive, why does the efficiency of microwave heating increase rapidly when steel slag is used? Liu *et al.* (2017) sought to test the electromagnetic properties of asphalt concrete with steel slag coarse aggregate to reveal the mechanism by which microwave heating efficiency is enhanced. Li *et al.* (2018) investigated the electromagnetic properties of steel slag filler and limestone filler to reveal the microwave heat release mechanism of the corresponding asphalt mastic. It is noteworthy that the above investigations either focus on the electromagnetic properties of the asphalt concrete as a whole or measure the electromagnetic properties of the microwave-absorbing components. The microwave absorption mechanisms among the components in complex asphalt-filler-aggregate systems have not yet been clarified. When exposed to microwave radiation, the mode of interaction between the bitumen and steel slag components, the electromagnetic properties of the individual components and the overall electromagnetic characteristics of the blend determine the overall microwave absorption response of the asphalt mixtures. Apparently, more scholars have focused on the evaluation of phenomenological indicators rather than a meticulous and in-depth study of the micro-mechanisms of interaction between steel slag filler/aggregate and bitumen. Besides, the microwave absorption mechanisms of the composites, particularly for asphalt mastic systems containing steel slag fillers, have also not been fully clarified as of now. There is little published literature on the critical topic of microwave absorption mechanisms of bitumen and steel slag filler systems. This paper will contribute more data on this topic in order to support the improved functionality of steel slag solid waste for pavement projects and to pave the way for the functional applications of steel slag in the asphalt industry.

The electromagnetic behaviour exhibited by a material depends on the inherent physical and chemical characteristics of the material. For this reason, it is necessary to first understand the characteristics of microwave-sensitive materials, their physical and chemical properties and the microscopic mechanisms of interaction within asphalt mixes. When steel slag powder replaces the natural fillers, the physico-chemical reactions between steel slag particles and bitumen, the microscopic mechanisms of interaction in composites are not yet clear, and this paper will provide some necessary mechanistic data for this purpose. The purpose of rapid rehabilitation technology is to extend the service life and service level of pavement projects. There is another characteristic, i.e. the fatigue endurance performance of steel slag-based asphalt materials, which also has an inherent effect on the fatigue life of asphalt pavements. This issue is crucial in assessing the fatigue durability of asphalt pavements constructed with steel slag components under the combined effects of vehicle loads and complex environments, and this property can be guaranteed at the design stage of the material ensemble. However, there is no unanimous conclusion on whether steel slag fillers can

improve the fatigue life of asphalt concrete, particularly the asphalt mastic phase, under cyclic loading. In this respect, this investigation aims to provide an in-depth and meticulous assessment work on the component interaction mechanisms, underlying electromagnetic mechanisms, microwave heating efficiency and stiffness response under cyclic testing for asphalt mastic containing steel slag fillers.

2. Objectives

There is no clear understanding of the functional design principles and mechanisms involved in rapid crack repair or deicing techniques in asphalt pavement layers under microwave irradiation. Current research and related reports are not sufficient to clearly reveal these application realities and potential mechanisms, and this is the rationale for this study, the primary objectives of which are as follows:

- to identify the chemical composition of steel slag fillers and the mechanisms of interaction between asphalt binders and different fillers.
- to determine the microwave absorption efficiency of composites containing SBS-modified bitumen and steel slag fillers.
- to shed light on the microwave absorption mechanisms of steel slag-based asphalt mastic in terms of dielectric characteristics and microwave penetration depths.
- to study the fatigue durability of steel slag-based asphalt mastic composites through stiffness characterisation and fatigue response under cyclic shear testing.

3. Materials and methodologies

3.1 Material and sample preparation

The SBS modified bitumen was prepared using a combination of a mechanical mixer and a high speed shear at a temperature of 170 °C as outlined in Figure 1 (Wang *et al.* 2020b). The filler powder, thoroughly dried, was added to the SBS modified bitumen and subjected to a high speed shearing for 20 min to obtain the asphalt mastic. The proportion of SBS copolymer in the bitumen is 4wt%. The penetration, ductility and softening point of the SBS modified bitumen at 25 °C are 5.8 mm, > 100 cm and 63 °C in that order. The physical features of the fillers used are given in Table 1. The steel slag powder was obtained by finely grinding weathered basic oxygen furnace (BOF) steel slag in a colloidal mill. In this research, the design ratio of bitumen-filler is by volume rather than by mass due to the different densities of steel slag powder and natural limestone powder, and the volume ratios chosen were 0.2, 0.3 and 0.4.

Table 1. Physical properties of fillers.

Technical index	Unit	Limestone filler	Steel slag filler
Hydrophilic coefficient	–	0.690	0.630
Density	g/cm^3	2.964	3.247
Water absorption rate	%	0.540	0.670
Specific surface area	m^2/g	1.430	1.960

3.2 Aging tests for asphalt mastic

The ageing effect of the climatic environment to which asphalt pavement materials are subjected cannot be neglected. The role of ageing considerations usually needs to be taken into account when evaluating the long-term performance. In this regard, the rolling thin-film oven tests (RTFOT) (ASTM D2872 2014) is a commonly employed test approach to simulate the short-term ageing effects suffered by asphalt materials and is followed in this study. An innovative methodology to simulate long-term ageing is the Ultraviolet (UV) ageing test, which focuses more on the photo-oxidative ageing effects in a natural climate and which helps to monitor the weathering and durability characteristics of asphalt materials. The UV radiation intensity on the mastic specimens was $150 w/m^2$, the temperature was 45 ± 5°C, and the UV aging period was 72 h. For more details on the parameters and settings of the UV ageing test, please refer to the previous research (Wang *et al.* 2022, Wang *et al.* 2021, Wang *et al.* 2020b).

3.3 Chemical and mechanism characterisation

3.3.1 Chemical composition analysis of fillers

X-ray fluorescence spectrometer (XRF, Panaco Epsilon3) was utilised to investigate the surface chemical composition of the steel slag filler and natural limestone filler. The steel slag aggregates and limestone fine aggregates were first ground to a powdery state using a ball mill, secondly the powder was screened through a 0.075 mm size sieve, and finally the screened powder was heated and dried in a drying chamber

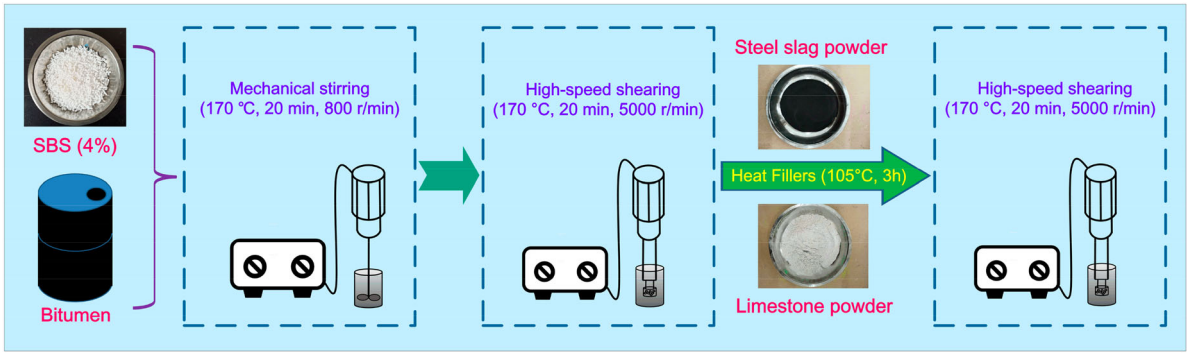

Figure 1. Schematic diagram of the preparation process of asphalt mastic.

at 105 °C for 3 h. 50 g of steel slag powder and limestone powder were selected for subsequent testing.

3.3.2 Characterisation of asphalt-filler interaction mechanism

Before investigating the application possibilities of a material, it is necessary to first gain an overview of the inherent characteristics of the material. Revealing the interaction mechanisms between SBS modified bitumen and steel slag filler and their microscopic mechanisms in turn contributes to illuminating the macroscopic characteristics. In this case, scanning electron microscope (SEM), X-ray diffraction (XRD), thermo gravimetric analyzer (TGA), and Fourier transform infrared (FT-IR) spectroscopy were adopted to measure the microscopic interaction mechanisms between bitumen and various types of fillers. The objectives of the SEM, XRD, TGA and FT-IR micro-testing methods are, in order of priority, the morphological characteristics, intercalation structure and crystallisation effect, thermal stability and chemical structural characteristics of the asphalt mastics containing steel slag fillers or natural limestone fillers. Details of the tests can be found in the literature (Wang *et al.* 2021, Cheng *et al.* 2011, Yin *et al.* 2017).

3.4 Microwave heating rate of asphalt mastics

The temperature response of the asphalt mastic after exposure to microwave radiation can distinguish the similarities and differences between SBS/steel slag-based asphalt mastic (SBS-SS) and SBS/limestone-based asphalt mastic (SBS-LS). Following the most innovative research methods already available (Li *et al.* 2018, Wang *et al.*, 2019b), the initial surface temperatures of the two types of asphalt mastic were measured and recorded using a HIKVISION infrared camera. The asphalt mastic samples were heated by microwave radiation using microwave heating device (Panasonic, Japan) with an output power of 800 W and a frequency of 2.45 GHz. A heating time period was 10 s and each sample was subjected to the same 10 continuous heating cycles. Between each two heating cycles, the microwave oven was switched on and the surface temperature distribution of the asphalt mastic was examined with the infrared camera, a process which took less time (not more than 5 s). Figure 2 visualises a schematic diagram of the microwave heated asphalt mastic.

3.5 Electromagnetic performance-dielectric measurements

3.5.1 Microwave heating fundamentals

When a material is irradiated and heated by microwaves, the amount of energy converted from electromagnetic field energy to heat within the substrate can be expressed in terms of the volumetric heat generation parameter Q (W/m^3), calculated as in Eq. 1.

$$Q = \omega \cdot \varepsilon''_{\text{eff}}(\omega) \cdot \varepsilon_0 \cdot E^2 \tag{1}$$

where ω is the angular frequency and is equal to $2\pi f$, f is the frequency, Hz; ε_0 denotes the vacuum permittivity (8.85×10^{-12} F/m); E refers to the applied external electric field (V/m); $\varepsilon''_{\text{eff}}(\omega)$represents the effective loss factor determined via Eq. 2:

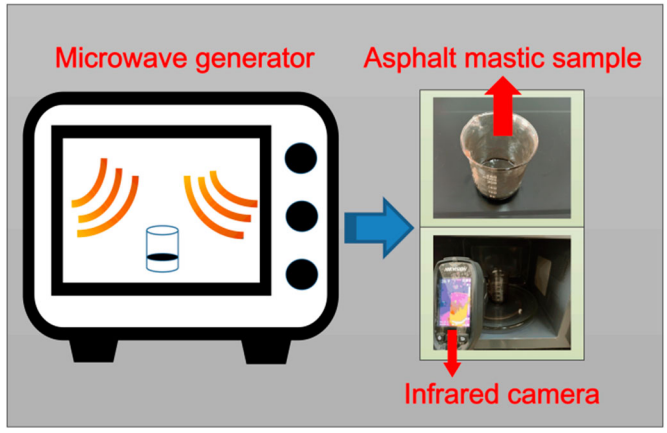

Figure 2. Microwave heating process for asphalt mastic samples (Wang *et al.*, 2022).

$$\varepsilon''_{\text{eff}}(\omega) = \varepsilon''_r(\omega) + \frac{\sigma}{\omega \cdot \varepsilon_0} \tag{2}$$

whereσstands for the conductive parameter of a material; $\varepsilon''_r(\omega)$ is the imaginary part of the complex relative permittivity $\varepsilon_r(\omega)$, also known as the loss factor which measures the consumption of electric field energy as well as the capacity to convert electric field energy into heat or thermal energy. Herein, $\varepsilon_r(\omega)$, which is a parameter describing the intrinsic relationship between the electric flux density and the electric field intensity in a loss medium, can be expressed as:

$$\varepsilon_r(\omega) = \varepsilon'_r(\omega) - j\varepsilon''_r(\omega) \tag{3}$$

where $\varepsilon'_r(\omega)$ is the real part of $\varepsilon_r(\omega)$ and indicates the capability of a dielectric material to store electric field energy and is also known as the dielectric constant. For non-magnetic dielectrics, the parameter $\varepsilon''_r(\omega)$ determines the heating characteristics and rate of heating of the dielectric under the effects of microwave irradiation. Thereby, the loss factor mentioned above is a critical parameter in determining the response of microwave radiation and heat conversion.

Another key variable to be mentioned is the penetration depth (D_P), which directly determines the depth of penetration of the microwave radiation within the volume of the dielectric material and the domain of influence. For quantitative analysis, the D_P parameter is known specifically as the depth to which the power flux density falls to 1/e of its surface. On the basis of available studies (Metaxas *et al.*, 1983, Peng *et al.*, 2010), the value of the penetration depth is related to the dielectric characteristics and the permeability properties of the material, and can be obtained via the Eq. 4:

$$D_P = \frac{\lambda}{2\sqrt{2}\pi}\{\varepsilon''_r\mu''_r - \varepsilon'_r\mu'_r + [(\varepsilon''_r\mu''_r)^2 + (\varepsilon'_r\mu'_r)^2 + (\varepsilon'_r\mu''_r)^2 + (\varepsilon''_r\mu'_r)^2]^{1/2}\}^{-1/2} \tag{4}$$

whereλdenotes the electromagnetic wavelength, numerically equal to c/f, and $c = 3.0 \times 10^8$ m/s; μ'_r and μ''_r represent the

real and imaginary parts of the complex relative permeability, respectively. Similar to the permittivity index,μ_r'measures the stored magnetic energy of a magnetic material and μ_r'' can be used to calculate the dissipation of magnetic field energy. Once neglecting the magnetic effects ($\mu_r'' = 0$), the equation for the depth of transverse electromagnetic mode power penetration of microwaves in materials with only a dielectric response can then be further simplified as:

$$D_P = \frac{\lambda}{2\pi(2\varepsilon'_r)^{1/2}} \left\{ \left[1 + \left(\frac{\varepsilon''_r}{\varepsilon'_r} \right)^2 \right]^{1/2} - 1 \right\}^{-1/2} \quad (5)$$

When $\varepsilon_r'(\omega)\backslash\mathrm{gg}\ \varepsilon_r''(\omega)$, D_p can be further simplified into the following form (Metaxas *et al.*, 1983, Angela *et al.*, 2012):

$$D_P = \frac{\lambda}{2\pi} \frac{\sqrt{\varepsilon'_r}}{\varepsilon''_r} \quad (6)$$

Through Eqs. 1–6, it is easy to find that the dielectric loss factor is positively correlated with heat, the larger the value of $\varepsilon_r''(\omega)$ means that the volume heat production of the material under microwave irradiation is greater; at the meantime, the dielectric loss factor is negatively correlated with the penetration depth, the larger the value of $\varepsilon_r''(\omega)$ results in a smaller D_p value.

In the available investigations by Liu *et al.* (2017) and Gulisano *et al.* (2021), based on the mineralogical characterisation, no trace of magnetite was found in the steel slag aggregates, and therefore they hypothesised that the contribution of magnetic losses to the heating in MW heating of electric furnace slag mixes is quite small and therefore negligible, while dielectric losses are the predominant contributor. On the one hand, given that conventional asphalt concrete is a non-magnetic material and the magnetic permeability properties of the material can be discounted. On the other hand, the magnetic susceptibility of the asphalt mastics with minor contents of steel slag fillers is not significant. Consequently, this study will focus on the investigation of the dielectric characteristics of the asphalt mastic containing steel slag fillers in order to reveal the electromagnetic response mechanisms underlying microwave radiation heating.

3.5.2 Dielectric measurements

The Agilent E5071C network analyzer and high-temperature coaxial probe kit were employed to test the dielectric behaviour and potential electromagnetic losses of asphalt mastics and fillers. It should be noted that the flatness of the specimen must be ensured. The test frequency range was 1GHz to 8GHz and the temperature was kept at ambient in a dry environment. The specific test details and methods are described in detail in the corresponding literature (Gulisano *et al.*, 2021, Zhai *et al.*, 2018). Herein, Figure 3 describes the schematic diagram of the high temperature coaxial probe technique for testing the dielectric properties of fillers and asphalt mastics.

3.6 Shear fatigue testing of asphalt mastic

3.6.1 Fundamental theoretical background

The viscoelastic continuum damage theory (VECD) model is a model for analysing the relationship between the decay of viscoelastic material models and the accumulation of damage to materials, and has undergone 30 years of development (Schapery, 1984; Park *et al.*, 1996; Lee *et al.*, 1998; Daniel *et al.*, 2002; Chehab *et al.*, 2003; Kim *et al.*, 2004; Underwood *et al.*, 2006; Kutay *et al.*, 2008; Underwood *et al.*, 2010; Zhang *et al.*, 2013; Sabouri *et al.*, 2014; Underwood, 2016). The damage model assumes that the damage behaviour of the material during loading and its evolution is due to the inherent characteristics of the material rather than the loading conditions and loading mode. The objective of quantifying damage is achieved by defining the change in internal state of the material during fatigue loading as the damage intensity. Depending on the category of work performed, there are two main types of approaches, one based on the pseudo strain energy method given by Park *et al.* (1996) and the other based on the dissipated energy (DE) density method proposed by Johnson (2010). A detailed description can be found in the

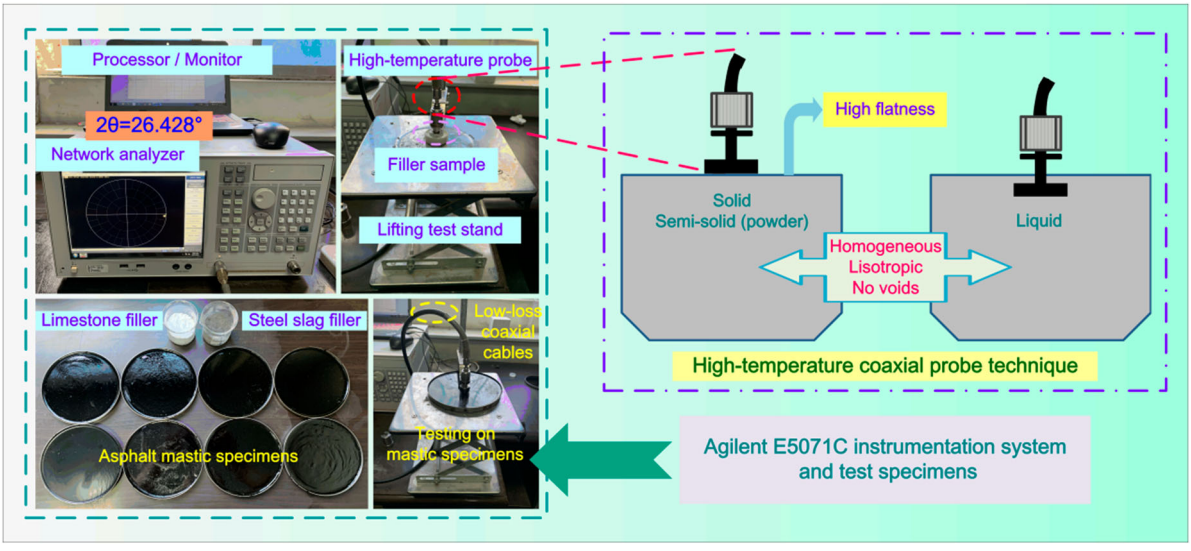

Figure 3. Schematic diagram of the high-temperature coaxial probe technique for testing the dielectric properties of fillers and asphalt mastics.

literature (Sun *et al.*, 2019). In this study, the DE density approach was adopted and the corresponding accumulated damage $D(t_N)$ of asphalts can be obtained via Eq. 7:

$$D(t_N) \cong \sum_{i-1}^{N} [\pi I_D \gamma^2 (G^*_{i-1} \sin\delta_{i-1} - G^*_i \sin\delta_i)]^{\frac{\alpha}{1+\alpha}} (t_i - t_{i-1})^{\frac{\alpha}{1+\alpha}} \tag{7}$$

where γ is the shear strain, G^* is the complex shear modulus, δ is the phase angle, here $ID = 1$ MPa, $\alpha = 1 + 1/m$, where the *m-value* was the slope of the fitted value of the main curve of the dynamic shear modulus of the material. As can be deduced from Eq. 7, the intensity of damage to a material can be characterised and measured in terms of dynamic mechanical response. Subsequently, the model can be fitted using the following equation (Johnson, 2010; Kim *et al.*, 2006):

$$G* \sin\delta = C_0 - C_1 (D)^{C_2} \tag{8}$$

where *C1* and *C2* are the fitting parameters, and $C0 = 1$.

Thereafter, a relationship between the fatigue life of asphalt cement materials and cyclic loading can be established for asphalt-based composites via Eq. 9:

$$N_f = A(\gamma)^{-B} \tag{9}$$

Where $k = 1 + (1 - C_2)\alpha$, and A and B are fatigue law parameters determined by Eqs. 10 and 11, respectively.

$$A = \frac{f\,(D_f)^k}{k(\pi I_D C_1 C_2)^{\alpha}} \tag{10}$$

$$B = 2\alpha \tag{11}$$

Hintz *et al.* (2011) demonstrated that the best correlations between the fatigue life values predicted by the linear amplitude sweep (LAS) test and the fatigue life obtained from the conventional fatigue tests measured were achieved when the $G^*\sin\delta$-value was decreased to 35% of the initial data. For this reason, a reduction in $G^*\sin\delta$-value to 35% of the initial data was selected as the fatigue failure criteria of asphalt materials in this study.

3.6.2 Fatigue tests

Firstly, the frequency sweep test was conducted at 10, 15, 20, 25 and 30 °C with a frequency sweep range of 0.1–100 rad/s and a strain level of 0.1%. This sweep was conducted to determine the linear viscoelastic rheological characteristics of the asphalt mastic and to obtain the input parameters of the model, i.e. the dynamic shear modulus. Secondly, the LAS tests (AASHTO, 2016) were conducted with a loading interval of 300 s at 10 Hz, a linear increase in amplitude from 0.1% to 30% and a test temperature of 25 °C. The fatigue tests are performed on the un-aged, RTFO-aged and UV-aged asphalt mastics containing steel slag fillers or natural limestone fillers.

4. Results and the main findings

4.1 Chemical analysis of steel slag and limestone fillers

As can be observed from the data in Tables 2 and 3, the principal chemical components of steel slag are Fe_2O_3, SiO_2 and CaO, whereas the principal components of limestone are CaO, SiO_2 and Al_2O_3, and the chemical composition of steel slag is of a more complex variety than that of limestone. The acidity of steel slag material can be obtained from the following equation:

$$M = \frac{CaO\%}{SiO_2\% + P_2O_5\%} \tag{12}$$

Accordingly, the alkalinity of the steel slag was calculated to be 0.288 and thus the slag itself is weakly alkaline based on the CaO, SiO_2 and P_2O_5 concentrations in the XRF test results. As bitumen is generally considered to be a weakly acidic material, the interaction between the steel slag filler and the bitumen under acid and alkali effects is significant.

4.2 Microscopic interactions between bitumen and fillers

4.2.1. Microscopic morphology

The microstructure of composite materials contributes to the identification of the internal distribution of the individual components of the material and helps to reveal the mechanisms of interaction between the individual components. Figure 4 gives an illustration of the microscopic morphologies of the fillers and the corresponding asphalt mastics. At a microscopic magnification of 500 times, tiny micropores are still visible on the surface of the fine steel slag powder particles. The natural stone still shows various prismatic shapes under the same test conditions, which is consistent with the results of the available literature (Pathak *et al.*, 2020). This phenomenon indicates that the surface morphology of the porous steel slag filler reflects the fineness and complexity of the pores within the steel slag when applied as coarse and fine aggregates. As described in Figure 4(c and d), the surface of the SBS/

Table 2. Chemical compositions of steel slag fillers.

Ingredients	Na_2O	MgO	Al_2O_3	SiO_2	P_2O_5	K_2O	CaO	SO_3	TiO_2
Content/%	2.468	2.578	7.574	29.033	0.211	1.000	8.431	0.197	0.426
Ingredients	V_2O_5	Cr_2O_3	MnO	Fe_2O_3	Co_3O_4	NiO	CuO	ZnO	As_2O_3
Content/%	0.010	0.225	0.920	40.111	0.207	0.018	1.273	2.171	0.255

Table 3. Chemical compositions of natural limestone fillers.

Ingredients	Na_2O	MgO	Al_2O_3	SiO_2	P_2O_5	K_2O	CaO	SO_3	TiO_2
Content/%	0.070	6.186	13.112	28.094	0.272	0.602	43.078	4.767	1.307
Ingredients	V_2O_5	Cr_2O_3	MnO	Fe_2O_3	Co_3O_4	NiO	CuO	ZnO	As_2O_3
Content/%	0.020	–	0.781	1.286	0.002	–	0.002	0.005	–

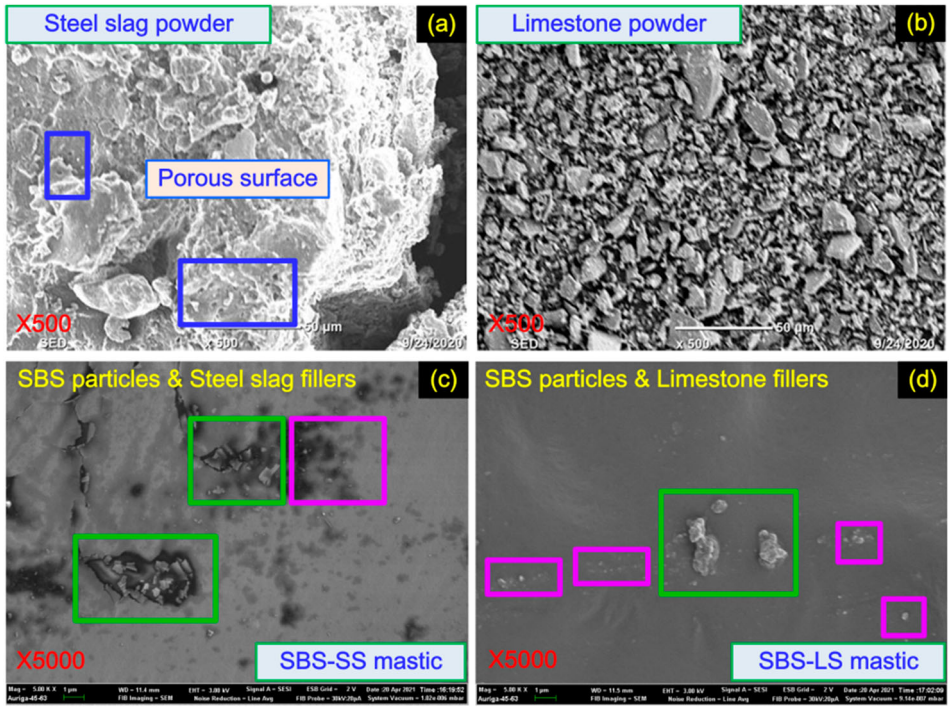

Figure 4. Microscopic morphology of fillers and the asphalt mastics.

limestone-based asphalt mastic was uneven and a more pronounced wrinkled structure could be observed, while the microscopic surface of the asphalt mastic with the same volume ratio of steel slag powder was flatter than that of the asphalt mastic with limestone fillers. Moreover, the SBS polymer particle-filler-bitumen blends exhibited various morphological characteristics as shown in Figure 4(c and d). The greater tendency of the steel slag filler to be coated by the SBS modified bitumen compared to the physical state of the limestone filler indicates better adhesion properties between the steel slag particles and the modified bitumen. This can be attributed to the structural properties of the porous steel slag particles and the greater adsorption of bitumen they produce.

4.2.2. XRD analysis

Figure 5 describes the XRD diffraction patterns of the control bitumen and two types of asphalt mastic, and Table 4 gives the XRD data of the diffraction peak location (2θ, °), interlayer spacing (d, Å), diffraction peak intensity (Area, mV· min), width (FWHM, °) and crystallite size (XS, Å). From the diffraction peak patterns and the data presented in Table 4, it is clear that after the addition of equal volume ratios of limestone powder and steel slag powder, the diffraction peak positions of

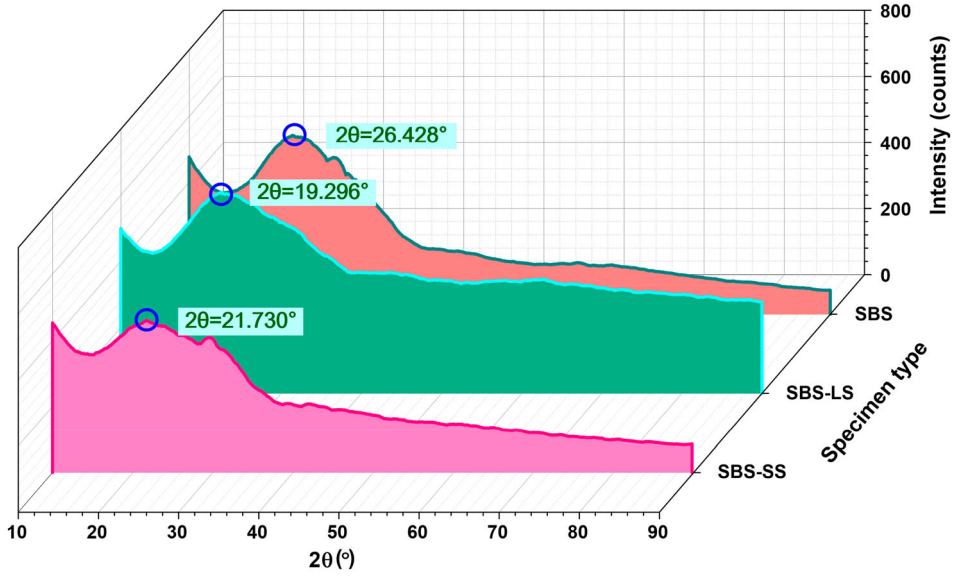

Figure 5. XRD diffraction patterns of asphalt mastics.

Table 4. XRD outcomes of the reference sample and asphalt mastics.

Sample ID	2θ (°)	d (Å)	Area (mV· min)	FWHM (°)	XS (Å)
SBS	26.428	3.369	11.60	0.133	930
SBS-LS	19.296	4.596	4.80	0.053	>1000
SBS-SS	21.730	4.086	12.40	0.142	800

both SBS-SS mastic and SBS-LS mastic changed, and the layer intervals of both SBS-SS mastic and SBS-LS mastic increased. This indicates that both steel slag and limestone particles can be incorporated into the crystal structure of SBS-modified bitumen (SMB) and that the resulting SMB-based mastic has a more stable intercalation-type crystal structure. In addition, the area data demonstrate that the diffraction peak intensity of the SBS-LS mastic was greater than that of the reference group of SBS modified bitumen. The intensity of the diffraction peaks of the SBS-SS mastic decreased in comparison to that of the reference group. This phenomenon indicates that the crystallinity and crystalline phase content are in the following order: SBS-SS > SBS > SBS-LS. Apart from this, the FWHM and XS data show that the steel slag causes an increase in the width of the diffraction peak and a decrease in the crystal size of the SMB. This indicates a more refined crystal structure of the SBS-SS mastic, whereas the SBS-LS asphalt mastic exhibits the opposite result.

4.2.3. Thermal stability analysis

Thermogravimetric (TG) and derivative thermogravimetry (DTG) curves of the SBS-SS mastic and the SBS-LS mastic are displayed in Figure 6. Herein, three parameters, namely the initial mass loss temperature (initial decomposition temperature, IDT), the maximum thermal decomposition temperature (T_{max}) and the final mass residual ratio can contribute to the assessment of the thermal stability of a bituminous mastic material. As depicted in Figure 6, the IDT temperature values indicate an initial decomposition onset temperature of 330 °C for SBS-SS, which is higher than the IDT values for SBS-LS and reference group SBS bitumen. For the T_{max} parameter, the values of SBS-SS, SBS-LS and control SBS are comparable, whereas for the residual ratio the results are SBS-SS > SBS-LS > SBS, indicating that SBS-SS asphalt mastic is more thermally stable than limestone-based asphalt mastic and polymer-modified bitumen.

4.2.4. FT-IR characterisation

The FT-IR analysis in this study was carried out to investigate, on the one hand, the chemical interactions between SBS modified bitumen and different types of fillers and, on the other hand, to assess the material response of both types of asphalt mastic to short and long-term ageing, particularly UV ageing. For the unaged specimens shown in Figure 7(a), compared to the reference group of SBS-based asphalt specimens, the characteristic peaks of the SBS-SS mastics and SBS-LS mastic became slightly sharper and had slightly different characteristic peaks in the range below 1000 cm^{-1}, attributed to the different chemical compositions of the steel slag filler and the limestone filler. In addition, the SMB sample and the SBS-SS mastic or SBS-LS mastic exhibited more pronounced characteristic peaks around 2920, 2850, 1600, 1460 and 1370 cm^{-1} respectively, which were mainly caused by the stretching vibration of the antisymmetric methylene CH_2 group, the stretching vibration of the symmetric methylene CH_2, the vibration of the symmetric C = C skeleton, bending vibrations of anti-symmetric methyl CH_3 and bending vibrations of symmetric methylene CH_3-functional groups. In addition, the SBS modified bitumen and the SBS-SS mastic both show more distinctive characteristic peaks around 966 and 698 cm^{-1} respectively, which are mainly owing to the out-of-plane bending vibrations of trans-C-H alkenes and cis-C-H alkenes. From Figure 7(b), it can be seen that after a short term ageing period, the characteristic peaks of the reference group asphalt, SBS-SS and SBS-LS asphalt pastes did not undergo any significant changes in the range of 1370–2930 cm^{-1}. The characteristic peaks emerged around 1030 cm^{-1}, mainly due to the stretching vibrations of the sulphoxide group S = O. The characteristic peaks were observed in the range of 720–900 cm^{-1}, mainly due to the out-of-plane bending vibrations of the benzene ring substituent after a short period of thermal oxidative ageing. As can be observed in Figure 7(c), the characteristic peaks of the reference group asphalt and the two asphalt mastics did not exhibit any significant changes in the ranges of 1030–2850 cm^{-1} and 720–900 cm^{-1}. The intensity of the characteristic peaks increased after the accelerated UV ageing procedure.

4.3 Microwave heating efficiency of asphalt mastic

The microwave heating efficiency of bituminous mastics can be characterised qualitatively and quantitatively in the laboratory, and the quantitative characterisation of the heat absorption efficiency of the materials is usually carried out at 2.45 GHz microwave equipment. This paper focuses on the microwave radiation response of SBS-SS and SBS-LS mastic

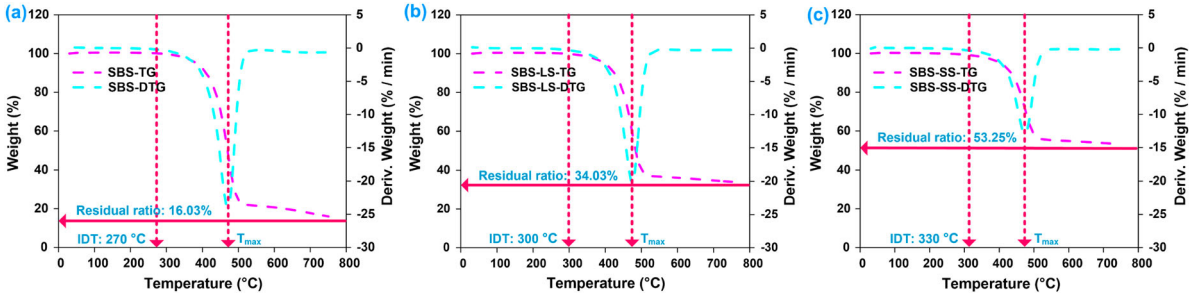

Figure 6. TG and DTG curves of asphalt mastics.

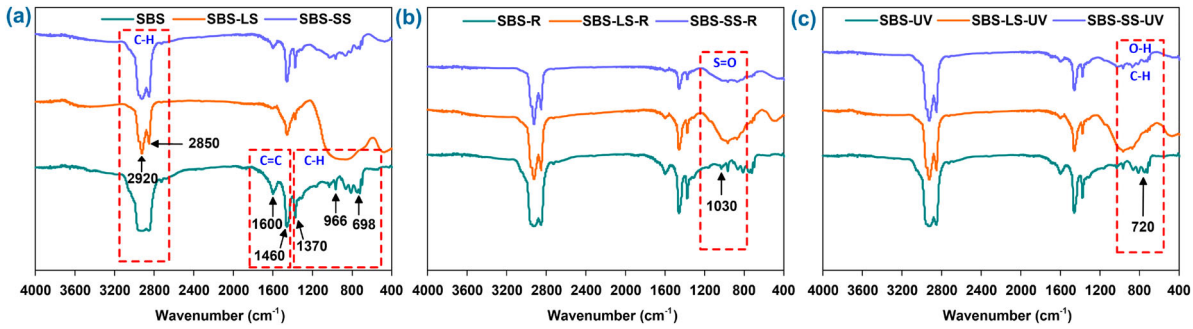

Figure 7. FT-IR spectra of the reference asphalt and asphalt mastic under three aging conditions.

materials at 2.45 GHz. The temperature rise tendencies of the reference group asphalt specimens, SBS-SS and SBS-LS asphalt mastic specimens under microwave irradiation are presented in Figure 8. A linear fit of the temperature change data points revealed that the correlation coefficient between the value of the temperature rise on the sample surface and the time of microwave irradiation, i.e. the R^2 value. The R^2 value was in the range of 0.96–0.99, implying a uniform and steady temperature rise of the asphalt mastic specimens. In order to specifically quantify the heating rate of a sample, a parameter, HR (°C/s), is introduced to characterise the heating rate of the material. Herein, the heating efficiency of asphalt mastics in a given time period of microwave irradiation was determined by $HR = \Delta T_i/\Delta t_i$, where $\Delta T_i$and Δt_i denote the temperature change and heating time interval within the i-th heating cycle, respectively. The outcomes in Table 5 suggested that the average heating rates of both steel slag-based and limestone-based asphalt mastics were generally greater than those of the reference group asphalt over the overall 100 s time period. The heating efficiency of the asphalt mastics containing steel slag powders was greater than that of the SBS-LS mastics with the same proportion of filler. For the same volume ratios of 0.2, 0.3 and 0.4, the increase in heating efficiency of SBS-SS over SBS-LS was 41.7%, 145.2% and 130.9%, in that order. Furthermore, the higher SS filler content further enhanced the heat absorption efficiency of the asphalt mastic composites, which is consistent with the findings of Wang *et al.* (2019a). Given that pure bitumen does not absorb microwaves, the reason why the temperature of the bitumen mastic composite increases after microwave irradiation is due to the filler and trace amounts of moisture. Previous XRF chemical fractions have demonstrated that steel slag fillers containing more iron oxide have the advantage and potential to absorb more electromagnetic waves than natural mineral stones.

4.4 Electromagnetic properties of fillers

Figure 9 shows the dielectric constant index and loss factor index of the fillers as a function of frequency (1–8GHz). The dielectric constant of the limestone filler fluctuates less with frequency and is stable in the range of 2.6–3.1. The dielectric constant of steel slag filler is higher than that of limestone filler due to high content of metal oxides such as ferric oxide, and the dielectric constant of steel slag filler is in the stable range of 4.6–5.0. As illustrated in Figure 9(b), the loss factor exhibited a fluctuating trend with frequency. Since the imaginary part of the relative complex permittivity of the material is generally lower, the difference between the two fillers in the imaginary part is much smaller than the difference in the real part. For the loss factor, the values tested for the steel slag filler are greater than those tested for the limestone filler in the lower frequency band (1–4 GHz), closer to those

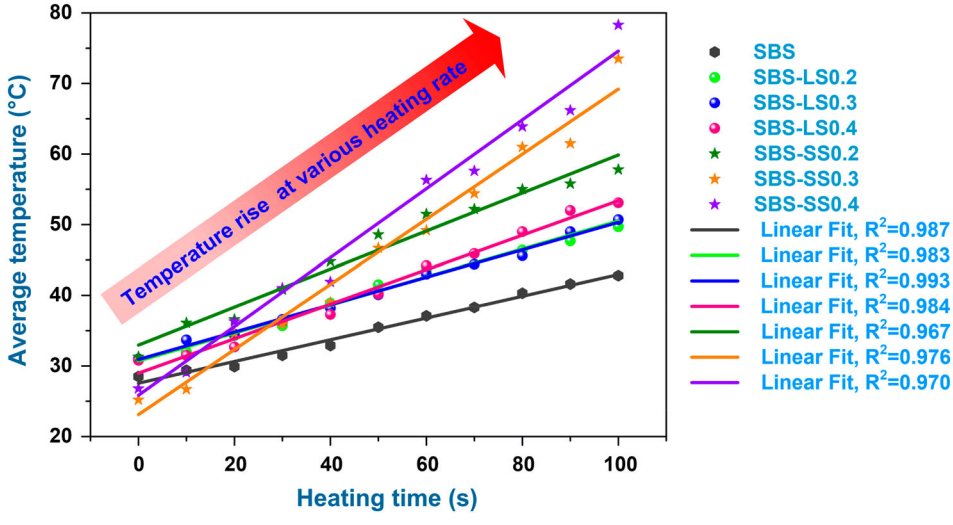

Figure 8. Temperature rises under microwave irradiation at 2.45 GHz.

Table 5. Average heating rate statistics for asphalt mastic.

Specimen ID	Fitting equations	R^2	Average heating rate (HR, °C/s) First 50s	Last 50s	Total time 100s
SBS	Y = 0.154x + 25.559	0.987	0.140	0.146	0.143
SBS-LS0.2	Y = 0.198x + 30.714	0.983	0.210	0.164	0.187
SBS-LS0.3	Y = 0.194x + 30.918	0.993	0.182	0.212	0.197
SBS-LS0.4	Y = 0.244x + 28.977	0.984	0.188	0.258	0.223
SBS-SS0.2	Y = 0.269x + 32.955	0.967	0.346	0.184	0.265
SBS-SS0.3	Y = 0.461x + 23.105	0.976	0.430	0.536	0.483
SBS-SS0.4	Y = 0.488x + 25.841	0.970	0.564	0.466	0.515

tested for the limestone filler in the intermediate frequency band (4–6 GHz) and greater than those tested for the limestone filler in the higher frequency band (6–8 GHz). The outcomes of the dielectric constants and loss factors of the fillers demonstrate that not only is the electric field energy storage capacity of the steel slag powder better than that of the limestone powder in this frequency band, but also the ability to transform electric field energy into thermal energy is superior to that of the limestone powder.

At the meantime, the findings of the chemical composition analysis revealed that the steel slag material employed in this study is free of magnetic ferrous oxide. The previous XRF chemical composition analysis findings revealed that the steel slag material employed in this study is free of magnetic ferrous oxide. Consequently, the electromagnetic losses of the asphalt mastic in this paper can be neglected for magnetic losses. Hence, when magnetic losses are not taken into account, the electromagnetic losses in non-magnetic materials are dominated by dielectric losses. The dielectric loss factor describes how much microwave energy is consumed by the filler through dielectric loss, expressed by the loss tangent angle (tan δ), which is numerically equal to $\varepsilon''/\varepsilon'$. The test results of the dielectric loss factor tan δ of the filler are presented in Figure 10. At the 2.45 GHz microwave frequency employed in this investigation, the dielectric loss factor of the steel slag filler is greater than that of the limestone filler. Furthermore, the tan δ outcomes further indicate that the steel slag powder consumes more microwave energy than the limestone.

4.5 Electromagnetic properties of asphalt mastic

The variation patterns of dielectric constant and loss factor for SBS-SS and SBS-LS mastics containing different filler to-bitumen volume ratios at the tested frequency bands are exhibited in Figures 11 and 12, respectively. The magnitudes of the dielectric constants of the asphalt mastics are remarkably smooth and do not fluctuate as much as the magnitudes of the loss factors. Within the test frequency range of 1 GHz to 8 GHz, the dielectric constant of the asphalt mastic raises with the growth of the filler-bitumen volume ratio. The greater the filler volume ratio, the greater the dielectric constant of the asphalt mastic. In the meantime, the loss factor behaves in the same way, i.e. an increase in the volume ratio of filler to bitumen enhances the loss factor of the asphalt mastic. For SBS-SS mastics the values of parameter$\varepsilon'$are roughly in the range of 3.0–4.0, while for SBS-LS mastics the value of parameter$\varepsilon'$is roughly 2.2–3.2. In addition, the average ε' of the SBS-SS mastic is always greater than the average value of SBS-SS mastic for the same filler-bitumen volume ratio. The results of the loss factor i.e. ε' parameter shown in Figure 11(b) and Figure 12 (b) are quite low and the maximum value does not surpass 0.3. As the frequency increases, the ε' parameter as a whole first tends to decrease and then gradually stabilises, although the values are widely scattered in the range 0.0–0.3.

The dielectric constants of the various asphalt mastics were averaged over the range of test frequencies by calculating the measured values for 200 data points, and the results are presented in Table 6. The standard deviations of the SBS-SS and SBS-LS asphalt mastics fluctuated in the range of 0.120–0.187 and 0.157–0.208 respectively. It is evident that the average dielectric constants of the asphalt mastics with different filler-bitumen volume ratios are relatively poorly discrete and less frequency dependent in the test frequency scope of 1 GHz to 8 GHz. The average dielectric constants of the asphalt mastic were analyzed as a function of the filler-bitumen volume ratio and the results are illustrated in Figure 13. The average ε'values for both types of asphalt mastic were found

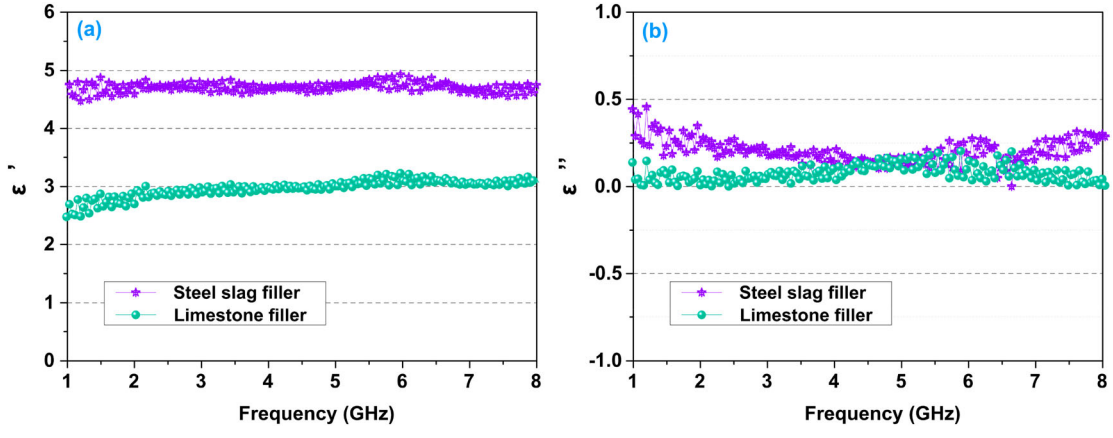

Figure 9. Dielectric constant and loss factor of fillers.

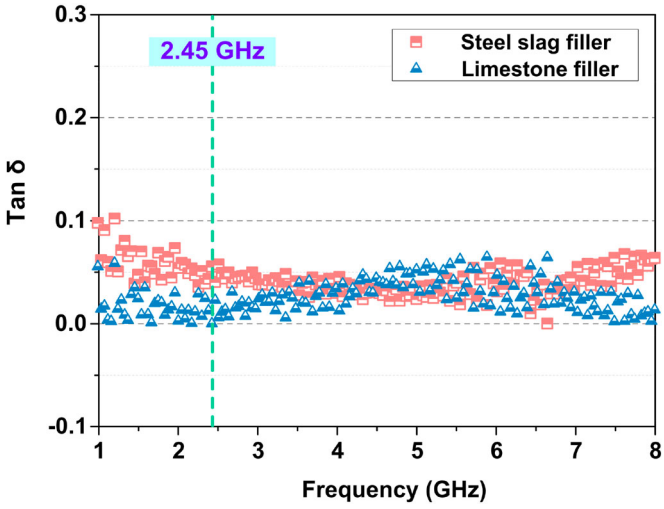

Figure 10. Measurement results for dielectric loss factor of fillers.

to grow as the filler-bitumen volume ratio increased. The average ε' of the SBS-SS asphalt mastic is greater than that of the SBS-LS asphalt mastic with the same filler-to-bitumen ratio. As a result, the permittivity of asphalt mastic is susceptible to the influence of the volume fraction of the components and their permittivity.

Nevertheless, as mentioned above, the dielectric loss factor tan δ is a vital parameter when using microwave heating techniques. It is utilised to characterise the microwave energy consumed by the asphalt mastic when only dielectric losses occur. The dielectric response for the parameter tan δ versus frequency is illustrated in Figure 14. In general, the values of the tan δ index of the SBS-SS and SBS-LS pastes are somewhat discrete, but they also exhibit an overall regularity. The dielectric loss factor tends to be greater for asphalt mastics containing higher volume rates of filler under the same frequencies, especially in the mid and low frequency bands. Comparing the two plots in Figure 14(a and b), it can be noticed that the overall improvement in dielectric loss of SBS-SS mastics compared to SBS-LS mastics is not outstanding probably due to the small magnitude of the loss factorε''. Nevertheless, the values of the dielectric loss of SBS-SS mastic are not the equal to those of SBS-LS mastic for a specific frequency such as 2.45 GHz or 5.8 GHz in engineering applications. With regard to the permittivity and dielectric loss of the asphalt mastic, the steel slag filler is superior to the limestone filler in terms of dielectric storage capacity and dielectric loss. For this reason, the microwave absorption capacity and heating characteristics of the steel slag-based asphalt mastic were found to be superior, thus validating the test findings in section 4.3 of this research.

4.6 Penetration depth (D_p)

It is preferable that the depth of penetration is equal to the thickness of the material in order to ensure the uniformity of microwave heating and the high efficiency of the absorbed energy. In practical applications, 2.45 and 5.8 GHz are the most widely available microwave frequencies (Gulisano *et al.*, 2021). The penetration depths corresponding to 2.45 and 5.8 GHz of the control asphalt and asphalt mastics were determined by Eq. 5, and the D_p values are shown in Figure 15. The penetration depth of the microwave in the asphalt mastic is lower than in the pure SMB, indicating that the addition of fillers reduces the penetration depth of the microwave in the interior of the asphalt matrix. The penetration depths of the SBS-SS mastic at 2.45 GHz were 0.231, 0.113 and 0.102 m in that order with filler-bitumen volume ratios of 0.2, 0.3 and 0.4, which were greater than the penetration depth results at 5.8 GHz. The microwave penetration depth of the limestone asphalt mastic also follows this trend at both two frequencies. Higher frequencies correspond to lower penetration depth values. The penetration depths of the SBS-SS mastics are lower than those of the SBS-LS mastic with the same filler-bitumen ratio under the same microwave radiation frequency. The low penetration depth corresponding to the high frequency is more suitable for snow and ice removal from pavements. The high penetration depth corresponding to the low frequency is more applicable to the rehabilitation of cracks in pavements. Low penetration depths mean that energy is converted quickly under microwave radiation and that the material has a greater potential to absorb microwaves. In terms of reasonableness, the 5.8 GHz frequency is more suitable for microwave heating for deicing operations and this view is consistent with the findings of

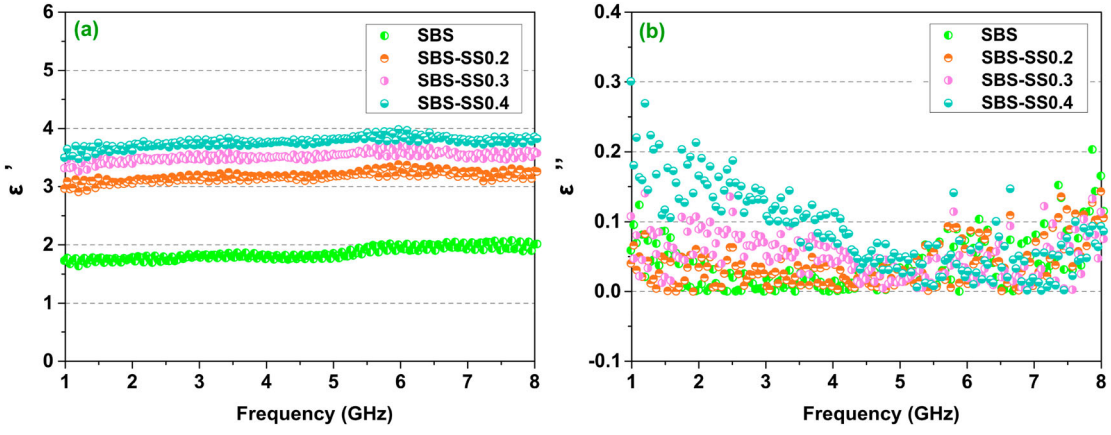

Figure 11. Dielectric constant and loss factor of the SBS-SS mastic.

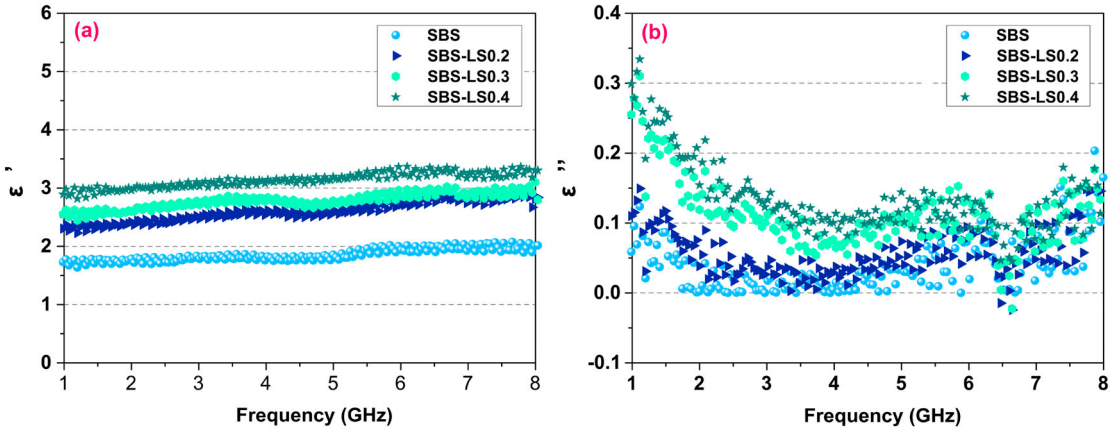

Figure 12. Dielectric constant and loss factor of the SBS-LS mastic.

Ding *et al.* (2018). Although 2.45 GHz is more suitable for the pavement maintenance operations, yet it is not chosen because of the high energy consumption (Gulisano *et al.*, 2021).

As mentioned above, when using microwave heating technology, the loss factor$\varepsilon''$is a vital parameter to characterise the capabilities of a material to convert electromagnetic energy into thermal energy. The reference group SBS-binder presents the greatest depth of penetration and the weakest loss factor when compared to the asphalt mastic specimens. As depicted in Figure 16, the loss factors of the material at 5.8 GHz are greater than those of the material at 2.45 GHz for both SBS-SS and SBS-LS mastics. In addition, the loss factors of SBS-SS mastics are generally greater than those of natural limestone-based asphalt mastics. Consequently, the utilisation of steel slag in road construction is highly feasible and recommended. Steel slag can generate more heat and thus enhance the energy efficiency of the microwave heating applications. In conclusion, with regard to the penetration depth and loss factor results, the lower penetration depth and higher loss factor of the asphalt mastic at 5.8 GHz compared to the 2.45 GHz application scenario. This phenomenon implies that the steel slag-asphalt based material is more capable of absorbing electromagnetic waves and therefore heats up faster resulting in saving pavement maintenance time in practical applications. The results are in agreement with the previous observations of Tang *et al.* (2008). Clearly, steel slag materials have an advantage over natural minerals in this respect.

4.7 Fatigue performance predictions of asphalt mastic

4.7.1 Linear viscoelastic characteristics

Figure 17 illustrates the dynamic shear modulus (G^*) master curves for asphalt mastics containing SBS modifiers and fillers, which can provide a better insight into the stiffness evolution pattern of the asphalt mastics in linear viscoelastic range. Specifically, Figure 17 presents the G^* curves for asphalt mastic specimens with different degrees of ageing, determined on the basis of the time-temperature superposition principle. The dynamic shear modulus of the reference group SBS, SBS-SS and SBS-LS mastics after short-term ageing was generally greater than that of the unaged asphalt mastic specimens described in Figure 17(a). For the long-term UV-aged samples shown in Figure 17(c), the dynamic shear modulus was slightly decreased rather than further improved from the short-term ageing level with the G^* response depicted in Figure 17(b). At all three levels of ageing, the largest dynamic modulus response values were observed for the SBS-SS mastic, followed by the SBS-LS mastic and the smallest for the reference group of SBS modified bitumens. Furthermore, the master curve tends to shift upwards, indicating an increase in the dynamic modulus as the filler-bitumen volume ratio increases.

Table 6. Numerical statistics of the average dielectric constants of reference group and asphalt mastics.

	SBS		SBS-LS		SBS-SS	
Filler-bitumen volume ratios	Average ε′	S.D.	Average ε′	S.D.	Average ε′	S.D.
0	1.861	0.128	–	–	–	–
0.2	–	–	2.583	0.208	3.147	0.147
0.3	–	–	2.771	0.162	3.502	0.120
0.4	–	–	3.122	0.157	3.733	0.187

4.7.2 Shear stress-strain responses

The stress-strain responses of the reference specimens and asphalt mastics were measured and recorded by standard LAS procedure. As shown in Figure 18(a), the peak shear stress

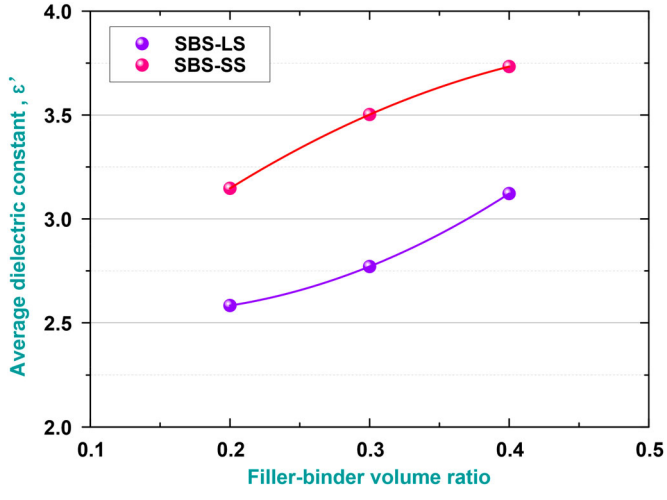

Figure 13. Relationships between the average ε' and the filler-bitumen volume ratio.

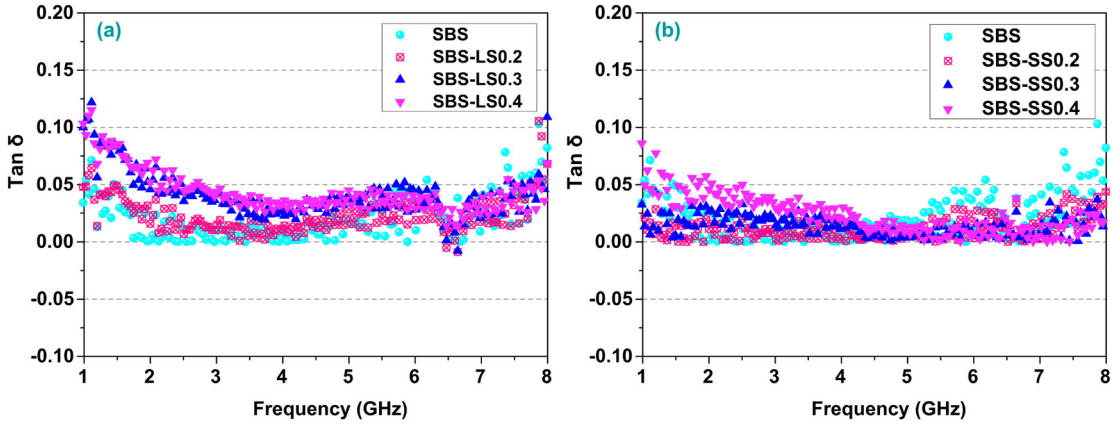

Figure 14. Dielectric loss factor tan δ versus frequency of the asphalt mastics.

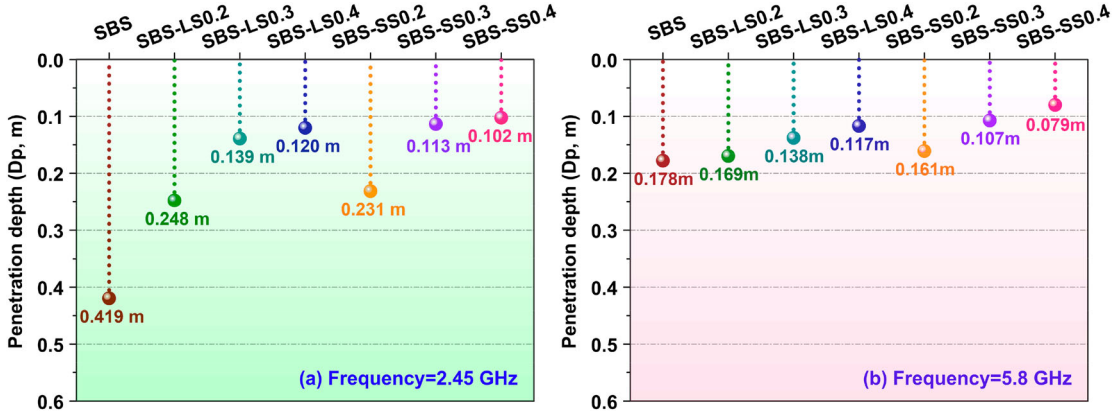

Figure 15. Penetration depths in asphalt mastic at application frequencies

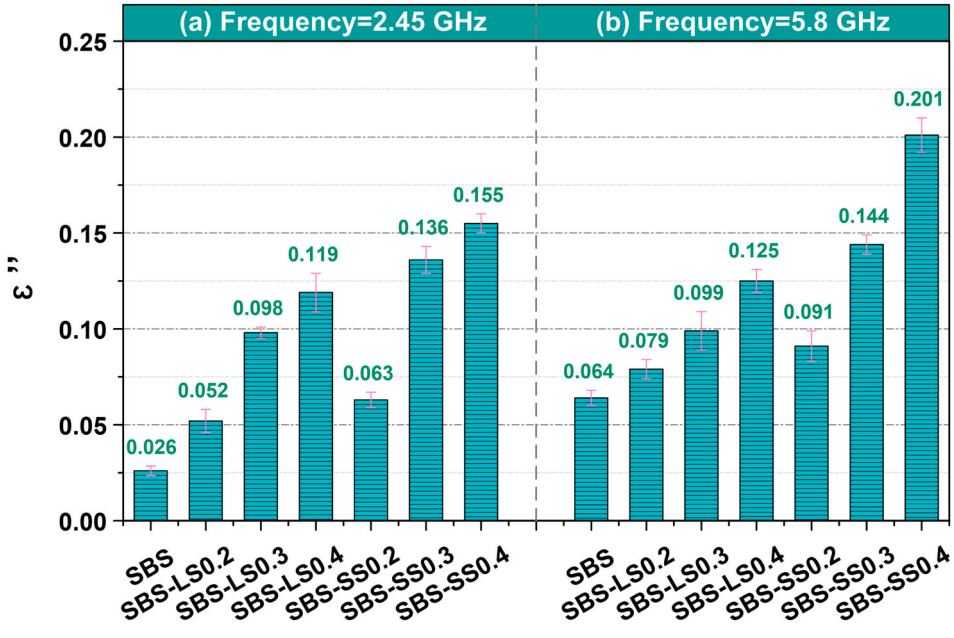

Figure 16. Loss factor of the asphalt mastic at application frequencies

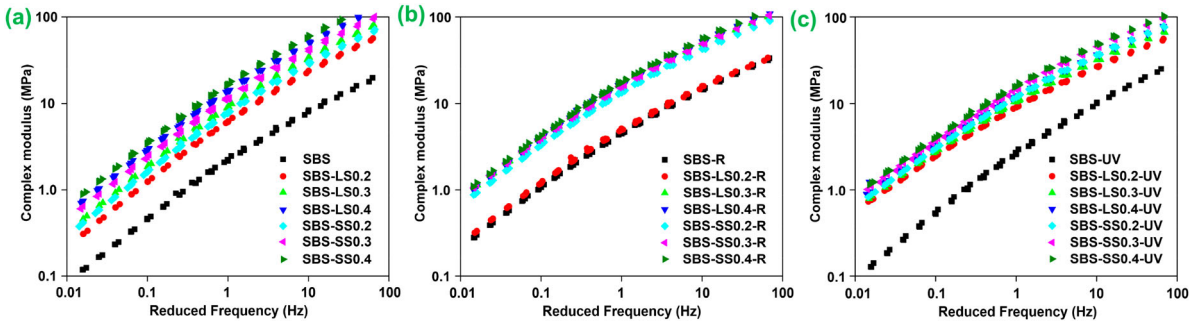

Figure 17. *G** master curves of the reference specimens and asphalt mastics.

of the SBS-SS mastic gradually grows as the steel slag filler increases, as does that of the SBS-LS mastic. The investigations by Sun *et al.* (2019) and Wang *et al.* (2018) concluded that a wider peak shear stress width means that the asphalt material is more resilient to deformability. However, the results in Figure 18 show that the peak shear stress widths of both the slag-based and limestone-based asphalt mastics tend to become narrower as the filler-bitumen volume ratio increases. This implies that the deformation resistance of the SMB is weakened by the addition of these two types of fillers. The peak shear stress of the short-term aged asphalt mastic specimens is greater compared to the original asphalt mastic specimens, but only for the low filler-bitumen volume ratio. However, the peak shear stress is even slightly lower for the 0.4 admixture ratio, as is the case for the short-term aged SBS-SS specimen. For the reference group of SBS modified bitumen, the peak shear stresses of both short and long term aged specimens were larger than the original specimens. The width of the peak shear stresses of the UV aged specimens was smaller than that of the original specimens, implying that UV aging reduced the deformation resistance of the bitumen modified by SBS co-polymers. As for the stress-strain responses of the UV-aged SBS-SS and SBS-LS mastics, there is a lack of significant describable regularity, suggesting that the components within the material that can resist shear deformation are more affected by photo-oxidative ageing.

4.7.3 Fatigue life predictions

Values of |G*|·sin δ and the corresponding damage intensity were recorded as damage accumulated in the asphalt mastic during fatigue testing according to AASHTO TP 101 (2016). As described in Figure 19, the initial data of the |G*|·sin δ determined by the average undamaged |G*|·sin δ values from 0.1% strain interval vary with the asphalt material types. The outcomes suggest that the steel slag filler and limestone filler affect not only the initial value of the parameter |G*|·sin δ, but also the evolution of the dynamic shear modulus with damage accumulation. Furthermore, the proportion of filler mix also has an effect on the damage evolution rate of the asphalt mastic. For the unaged specimens in Figure 19(a), the damage characteristic curves for SBS-SS mastics are generally lower than those for SBS-LS mastics. At the same time, the damage evolution curves for limestone-based asphalt mastics tend to shift upwards as the proportion of limestone filler is increased, implying a rapid accumulation of damage. As suggested in Figure 19(b and c), both the short-term ageing and UV ageing processes had a noticeable effect on the initial value |G*|·sin δ and the trends of the damage characteristic curves compared to the unaged specimens. The results indicate a variation in the internal state characteristics of the asphalt mastic after being subjected to various ageing mechanisms.

The fatigue life of the reference samples, SBS-SS mastics and SBS-LS mastics at different loading levels was calculated via Eq. 7 based on the VECD theory. The findings in Figure 20 suggest that the fatigue life values for both SBS-SS and SBS-LS mastics are significantly lower than for the reference SMB group, and the outcomes for the RTFO-aged samples are similar. The fatigue life of the asphalt mastic exhibited a tendency to decrease with greater filler blending ratios. The fatigue life of the SBS-SS or SBS-LS mastic with a filler-bitumen volume ratio of 0.4 was the minimum at strain levels of 0.04, 0.07 and 0.1. The fatigue life of the unaged SBS-SS mastic is comparable to that of the SBS-LS mastic at the same filler dosing ratio, while the fatigue life of the short-term aged

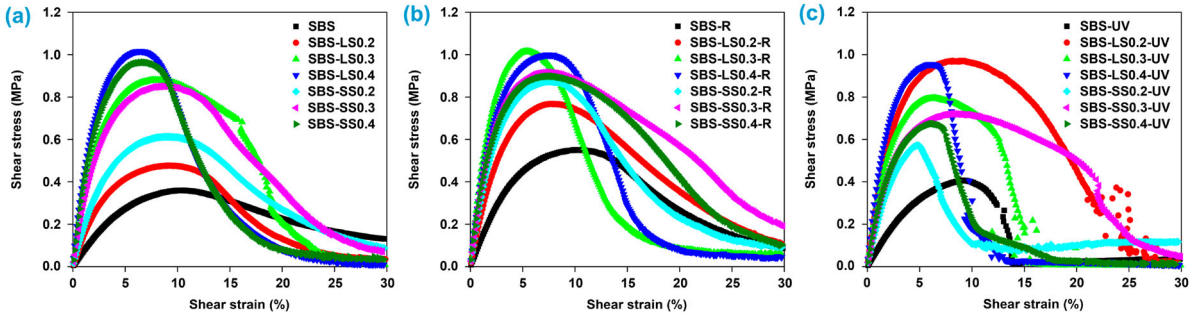

Figure 18. Stress-strain responses under standard LAS procedures.

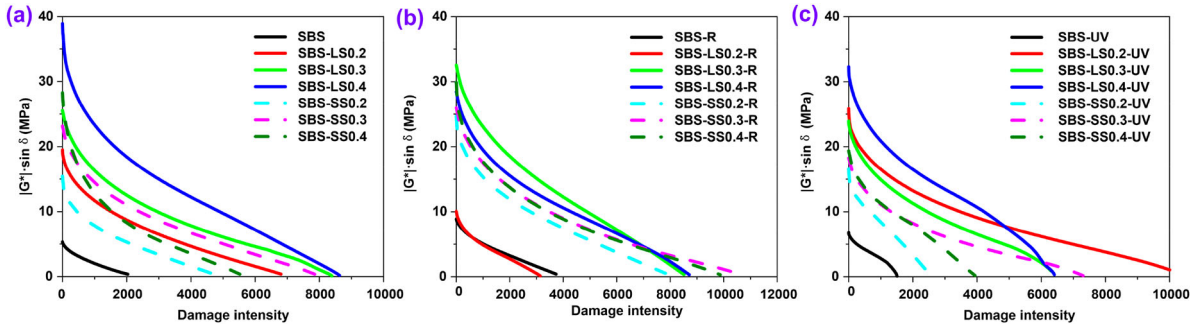

Figure 19. |G*|·sin δ versus damage intensity.

SBS-SS mastic is slightly higher than that of the SBS-LS mastic, as shown in Figure 20(a and b). For SBS-SS mastic and SBS-LS mastic, there was an overall increase in the values of RTFO-aged and UV-aged specimens compared to unaged specimens. Nevertheless, for the reference group of SBS modified bitumen, the fatigue life of the specimens was decreased after UV ageing. This indicates that the SBS bitumen specimens were more susceptible to UV ageing, possibly due to the degradation of the SBS polymer by UV exposure, resulting in a decrease in the internal elastic components.

To demonstrate more visually the variability of fatigue life for various asphalt mastic specimens, the values for fatigue life at a strain level of 0.1 are presented in Figure 21. The fatigue life predictions for the reference group of SMB specimens are the greatest for both unaged and RTFO-aged samples. In contrast, the fatigue life of SBS-SS and SBS-LS mastics drops with increasing filler volume ratios, implicating that steel slag fillers or limestone fillers reduce the ability of SMB to resist fatigue damage. Comparing Figure 21(a and b) it can be concluded that the short-term thermal oxidative ageing behaviour promotes the fatigue life of the reference group of SBS modified bitumen, SBS-SS mastic and SBS-LS mastic. The UV ageing data shown in Figure 21(c) illustrated that the predicted fatigue life of the reference group of SBS modified bitumen exhibited a substantial degradation, indicating a reduction in the fatigue resistance of the specimen after exposure to UV bursting. At this point, the fatigue life of the UV-aged SBS-SS and SBS-LS mastics was greater than that of the reference group specimens, and was also superior to that of the RTFO-aged specimens, particularly with a filler-bitumen volume ratio of 0.2.

4.7.4 Fatigue parameters A and B

The parameters A and B determined by Eq. 10 and Eq. 11 have been adopted to characterise the fatigue behaviour of asphalt materials. Parameter A represents the fatigue impedance and is employed to characterise the capability of a material against fatigue failure. Parameter B is referred to as the load sensitivity and is applied to characterise the sensitivity of a material to consecutive repetitive loading during fatigue testing. Table 7 shows the calculations of the parameters A and B for the reference sample and two types of asphalt mastic. For the un-aged asphalt specimens, parameter A tends to decrease with increasing filler content and is ranked as SBS modified asphalt > SBS-SS mastic > SBS-LS mastic at the same filler content. The phenomenon implies that the reference group specimens have higher fatigue impedance, which is line with the previous predicted fatigue life results. Moreover, the value of parameter B tends to decrease slightly with increasing filler, suggesting that steel slag filler and limestone filler can further decrease the load sensitivity of the SMB. The overall greater value of parameter A for RTFO-aged specimens compared to un-aged specimens indicates that short-term ageing has further enhanced the fatigue impedance of the asphalt and asphalt mastic. Consequently, the fatigue life of RTFO aged specimens exhibits a further growth trend as depicted in Figure 21(b). Most of the RTFO-aged specimens and UV-aged specimens exhibited an increasing trend in load sensitivity B-values compared to unaged asphalt specimens, with the exception of the UV-aged SMB specimens. Furthermore, the majority of UV-aged asphalt mastics displayed a decreasing trend in fatigue impedance A-values compared to RTFO-aged asphalt

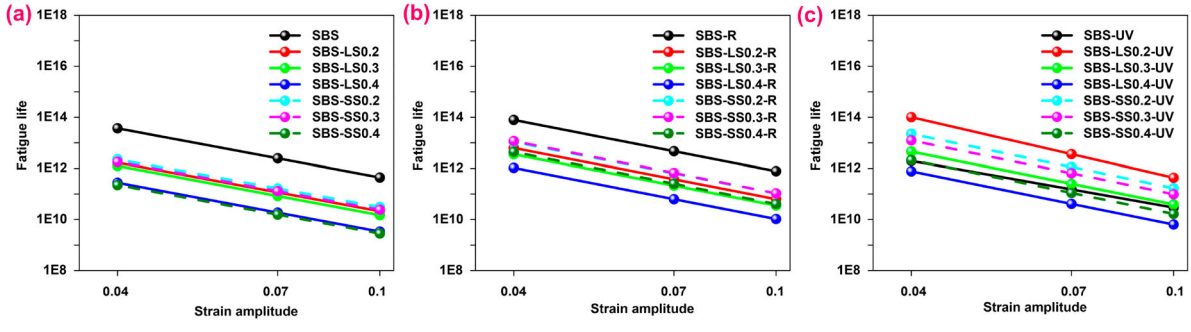

Figure 20. Fatigue life versus applied shear strain amplitude.

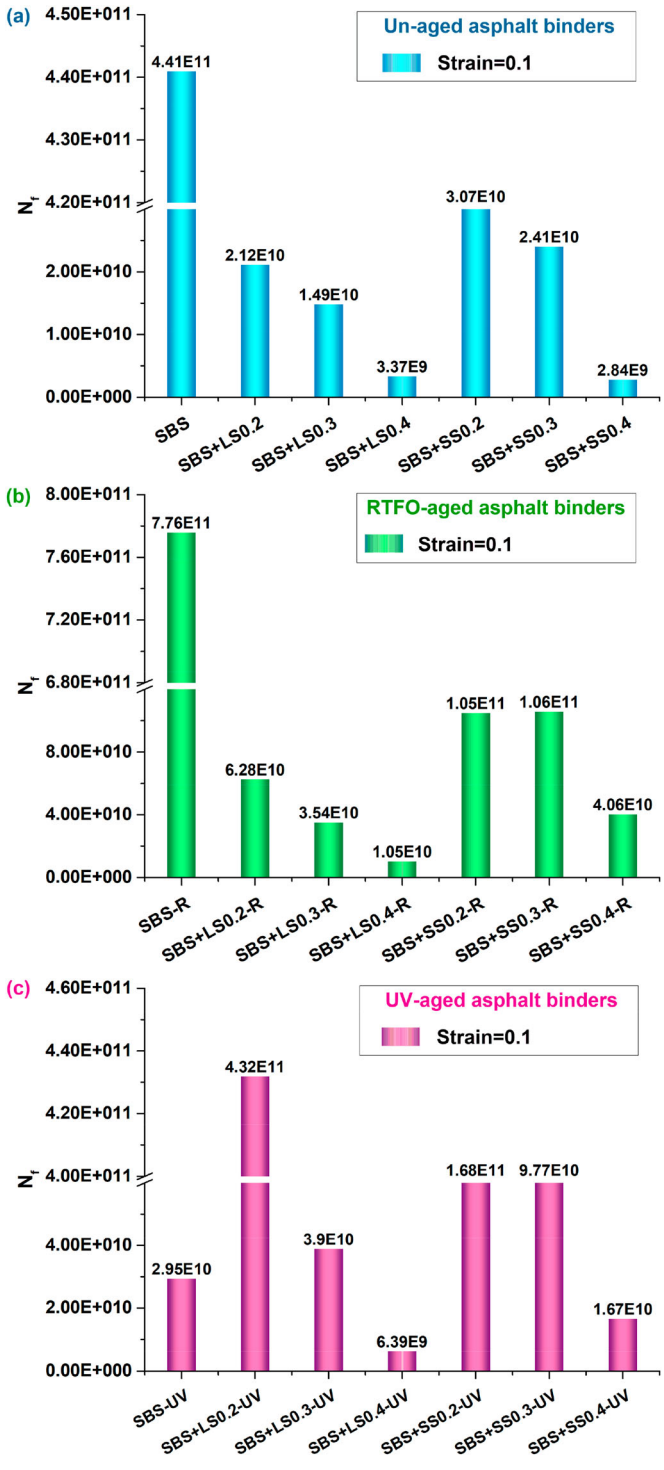

Figure 21. Predicted fatigue life for the asphalt mastic at 0.1 strain amplitude.

Table 7. A and B results for the reference sample and asphalt mastic.

	Un-aged		RTFO-aged		UV-aged	
Specimen ID	A	B	A	B	A	B
SBS	6459121	4.83	7055679	5.04	767708	4.58
SBS-LS0.2	357000	4.77	585514	5.03	483684	5.95
SBS-LS0.3	216626	4.84	324490	5.04	249882	5.19
SBS-LS0.4	52341	4.81	98223	5.03	38077	5.22
SBS-SS0.2	622851	4.69	912436	5.06	745346	5.35
SBS-SS0.3	465536	4.71	773292	5.14	500775	5.29
SBS-SS0.4	48192	4.77	75736	4.29	10361	4.70

specimens. This means that UV ageing further weakened the fatigue resistance of asphalt mastics that had undergone a short-term ageing process. However, this outcome exhibits the same scattered findings as in Figure 21(c) and appears to be independent of the volume ratio of the fillers.

5. Conclusions and recommendations

This study was to assess and compare the performance differences between steel slag filler and natural stone filler in terms of material characteristics, microwave heating efficiency and its underlying electromagnetic heating mechanisms, and fatigue durability characteristics. The following main conclusions were drawn:

- The surface morphology of the porous steel slag filler demonstrates the fineness and complexity of the pores within the steel slag when applied as coarse and fine aggregates. And it is the higher ferric oxide content that makes the electromagnetic wave energy absorption characteristics of steel slag material superior to those of natural stone. The crystallization effect and thermal stability of SBS-SS mastic are superior to those of SBS-LS mastic, and there are no distinctive peaks in the IR diffraction spectra of either type of asphalt mastic specimens after RTFO ageing and UV ageing.
- Steel slag fillers with higher iron oxide content have the advantage and potential to absorb more electromagnetic waves than the natural minerals. The average heating efficiency of SBS-SS mastics under microwave irradiation is significantly greater than that of the reference group of bitumen and natural stone based mastics.
- The steel slag filler is superior to the limestone filler in terms of dielectric storage capacity and dielectric loss. As a result, the electric field energy storage capacity and the potential to convert electric field energy into thermal energy of the steel slag filler and the corresponding SBS-SS mastic are significantly greater than those of the natural limestone filler and the corresponding SBS-LS mastic.
- The microwave penetration depth of the SBS-SS mastic is less than that of the SBS-LS mastic with the same filler-bitumen ratio at the same microwave radiation frequency. For this reason, the application of steel slag in the construction of functional pavements with microwave rapid repair performance is very feasible and recommended.
- The analysis of the fatigue life and fatigue impedance parameters revealed that the addition of steel slag filler and limestone filler weakened the deformation resistance and fatigue durability of the SBS modified bitumen.

This study sheds light on exploring the potential and benefits of steelmaking by-products, i.e. steel slag waste, in combination with microwave heating techniques in the functional pavement engineering industry. The microwave heating rate, electromagnetic loss characteristics and durability of asphalt concretes containing steel slag fine and coarse aggregates will be rigorously examined and demonstrated in the following research. The effects of individual components of asphalt concrete composites in terms of raw material

characteristics (steel slag source), void ratio, gradation, moisture content, physical and chemical attributes, and many other variables will also be considered. Furthermore, the coupling of the multi-physical effects of natural climate, heat transfer, electromagnetic fields and seepage fields should also be considered in the course of research in this research interest.

Acknowledgments

The financial supports from the Projects funded by China Postdoctoral Science Foundation (Grant No. 2021M692918), the Natural Science Foundation of Henan (Grant No. 222300420308), and the First-class Project Special Funding of Yellow River Laboratory (Grant No. YRL22YL05) were greatly appreciated.

Disclosure statement

No potential conflict of interest was reported by the author(s).

Funding

This work was supported by China Postdoctoral Science Foundation: [Grant Number 2021M692918]; Natural Science Foundation of Henan Province: [Grant Number 222300420308]; the First-class Project Special Funding of Yellow River Laboratory: [Grant Number YRL22YL05].

ORCID

Haopeng Wang http://orcid.org/0000-0002-5008-7322

References

AASHTO, 2016. Standard method of test for estimating damage tolerance of asphalt binders using the linear amplitude sweep, *AASHTO TP101*, Washington, DC.

Agzenai, Y., et al., 2015. Advanced self-healing asphalt composites in the pavement performance field: Mechanisms at the nano level and new repairing methodologies. *Recent Patents on Nanotechnology*, 9, 43–50.

Anastasiou, E.K., Liapis, A., and Papayianni, I., 2015. Comparative life cycle assessment of concrete road pavements using industrial by-products as alternative materials. *Resources, Conservation and Recycling*, 101, 1–8.

Angela, A., and d'Amore, M., 2012. Relevance of dielectric properties in microwave assisted processes. Microwave Materials Characterization, InTech.

ASTM D2872, 2014. *Standard test method for effect of heat and air on a moving film of asphalt (Rolling Thin-Film Oven Test)*. West Conshohocken, PA.

Barišić, I., Dimter, S., and Rukavina, T., 2014. Strength properties of steel slag stabilized mixes. *Composites Part B: Engineering*, 58, 386–391.

Chehab, G.R., et al., 2003. Characterization of asphalt concrete in uniaxial tension using a viscoelastoplastic model. *Asphalt Paving Technology*, 72, 315–355.

Chen, Z., et al., 2020. Moisture stability improvement of asphalt mixture considering the surface characteristics of steel slag coarse aggregate. *Construction and Building Materials*, 251, 118987.

Chen, X., et al., 2022a. Temperature analyses of porous asphalt mixture using steel slag aggregates heated by microwave through laboratory tests and numerical simulations. *Journal of Cleaner Production*, 338, 130614.

Chen, Z., et al., 2022b. Innovative use of industrially produced steel slag powders in asphalt mixture to replace mineral fillers. *Journal of Cleaner Production*, 344, 131124.

Cheng, I., et al., 2011. Synthesis of graphene paper from pyrolyzed asphalt. *Carbon*, 49, 2852–2861.

Daniel, J.S., and Kim, Y.R., 2002. Development of a simplified fatigue test and analysis procedure using a viscoelastic continuum damage model. *Asphalt Paving Technology*, 71, 619–650.

Ding, L., et al., 2018. Microwave deicing efficiency: study on the difference between microwave frequencies and road structure materials. *Applied Sciences*, 8 (12), 2360.

Fonseca, J., et al., 2019. Evaluation of effects of filler by-products on fine aggregate matrix viscoelasticity and fatigue-fracture characteristics. *Journal of Materials in Civil Engineering*, 31 (10), 04019240.

Gallego, J., et al., 2013. Heating asphalt mixtures with microwaves to promote self-healing. *Construction and Building Materials*, 42, 1–4.

Gallego, J., et al., 2021. The crucial effect of re-compaction energy on the healing response of hot asphalt mortars heated by microwaves. *Construction and Building Materials*, 285, 122861.

Gao, J., et al., 2017. Utilization of steel slag as aggregate in asphalt mixtures for microwave deicing. *Journal of Cleaner Production*, 152, 429–442.

García, Á., et al., 2009. Electrical conductivity of asphalt mortar containing conductive fibers and fillers. *Construction and Building Materials*, 23 (10), 3175–3181.

Guan, B., et al., 2019. Investigation of the microwave absorption of asphalt mixtures containing magnetite powder. *Coatings*, 9, 813.

Gulisano, F., et al., 2021. Dielectric characterisation of asphalt mortars for microwave heating applications. *Construction and Building Materials*, 308, 125048.

Hainin, M. R., et al., 2014. Performance of steel slag in highway surface course. *Jurnal Teknologi (Sciences & Engineering)*, 71 (3), 99–102.

Hainin, M. R., et al., 2015. Steel slag as a road construction material. *Jurnal Teknologi (Sciences & Engineering)*, 73 (4), 33–38.

Hasita, S., et al., 2020. Performance improvement of asphalt concretes using steel slag as a replacement material. *Journal of Materials in Civil Engineering*, 32 (8), 04020227.

Hintz, C., et al., 2011. Modification and validation of linear amplitude sweep test for binder fatigue specification. *Transportation Research Record: Journal of the Transportation Research Board*, 2207, 99–106.

Jiao, W., et al., 2020a. Study on thermal properties of steel slag asphalt concrete for snow-melting pavement. *Journal of Cleaner Production*, 277, 123574.

Jiao, W., et al., 2020b. Utilization of steel slags to produce thermal conductive asphalt concretes for snow melting pavements. *Journal of Cleaner Production*, 261, 121197.

Johnson, C.M., 2010. Estimating asphalt binder fatigue resistance using an accelerated test method. Dissertation (PhD). University of Wisconsin-Madison, Madison.

Kim, Y.R., et al., 2004. Dynamic modulus testing of asphalt concrete in indirect tension mode. Journal of Transportation Research Board. No. 1891, National Research Council. Washington D.C., 163–173.

Kim, Y., et al., 2006. A simple testing method to evaluate fatigue fracture and damage performance of asphalt mixtures. *Asphalt Paving Technology: Association of Asphalt Paving Technologists-Proceedings of the Technical Sessions*, 75, 755–788.

Kutay, M.E., Gibson, N.H., and Youtcheff, J., 2008. Conventional and viscoelastic continuum damage (VECD) based fatigue analysis of polymer modifed asphalt pavements. *Journal of Association of Asphalt Paving Technologists*, 77, 395–434.

Lee, H.J., and Kim, Y.R., 1998. Viscoelastic constitutive model for asphalt concrete under cyclic loading. *Journal of Engineering Mechanics*, 124 (1), 32–40.

Li, C., Wu, S., and Chen, Z., 2018. Enhanced heat release and self-healing properties of steel slag filler based asphalt materials under microwave irradiation. *Construction and Building Materials*, 193, 32–41.

Liu, X., et al., 2021. Improving the electromagnetic properties of bitumen using SiC-Fe_3O_4 composites. *Journal of Materials in Civil Engineering*, 33 (11), 04021326.

Liu, J., et al., 2022. Evaluation of self-healing properties of asphalt mixture containing steel slag under microwave heating: Mechanical, thermal transfer and voids microstructural characteristics. *Journal of Cleaner Production*, 342, 130932.

Liu, W., Miao, P., and Wang, S., 2017. Increasing microwave heating efficiency of asphalt-coated aggregates mixed with modified steel slag particles. *Journal of Materials in Civil Engineering*, 29 (10), 04017171.

Liu, X., Zhao, Y., and Zhang, D., 2020. Microwave absorption enhancement of asphalt concrete with SiC-Fe_3O_4 mixtures modifier. *Construction and Building Materials*, 254, 119209.
Lou, B., et al., 2020. Effect of metallic-waste aggregates on microwave self-healing performances of asphalt mixtures. *Construction and Building Materials*, 246, 118510.
Lu, S., et al., 2021. Research on electromagnetic properties and microwave deicing performance of carbon fiber modified concrete. *Construction and Building Materials*, 286, 122868.
Manso, J.M., et al., 2006. Durability of concrete made with EAF slag as aggregate. *Cement and Concrete Composites*, 28, 528–534.
Masoudi, S., Abtahi, M., and Goli, A., 2017. Evaluation of electric arc furnace steel slag coarse aggregate in warm mix asphalt subjected to long-term aging. *Construction and Building Materials*, 135, 260–266.
Metaxas, A.C., and Meredith, R.J., 1983. Industrial microwave heating. The Institution of Electrical Engineers, Peter Peregrinus, London, 80. AC Metaxas, RJ Meredith - 1983 - books.google.com.
Nadiatul Adilah, A. A. G., et al., 2020. The influence of steel slag as alternative aggregate in permeable concrete pavement. *Materials Science and Engineering Conference Series*, doi: 10.1088/1757-899X/712/1/012011.
Norambuena-Contreras, J., and García, Á., 2016. Self-healing of asphalt mixture by microwave and induction heating. *Materials & Design*, 106, 404–414.
Park, S.W., Kim, Y.R., and Schapery, R.A., 1996. A viscoelastic continuum damage model and its application to uniaxial behavior of asphalt concrete. *Mechanics of Materials*, 24 (4), 241–255.
Pasetto, M., et al., 2017. Sustainable solutions for road pavements: A multi-scale characterization of warm mix asphalts containing steel slags. *Journal of Cleaner Production*, 166, 835–843.
Pathak, S., Choudhary, R., and Kumar, A., 2020. Investigation of moisture damage in open graded asphalt friction course mixtures with basic oxygen furnace steel slag as coarse aggregate under acidic and neutral pH environments. *Transportation Research Record: Journal of the Transportation Research Board*, 2674 (8), 887–901.
Peng, Z., et al., 2010. Microwave penetration depth in materials with non-zero magnetic susceptibility. *ISIJ International*, 50 (11), 1590–1596.
Phan, T., Park, D., and Le, T., 2018. Crack healing performance of hot mix asphalt containing steel slag by microwaves heating. *Construction and Building Materials*, 180, 503–511.
Poulikalos, L.D., et al., 2017. Harvesting the unexplored potential of European waste materials for road construction. *Resources, Conservation and Recycling*, 116, 32–44.
Sabouri, M., and Kim, Y.R., 2014. Development of a failure criterion for asphalt mixtures under different modes of fatigue loading. *Transportation Research Record: Journal of the Transportation Research Board*, 2447, 117–125.
Schapery, R.A., 1984. Correspondence principles and a generalizedJ integral for large deformation and fracture analysis of viscoelastic media. *International Journal of Fracture*, 25 (3), 195–223.
Skaf, M., et al., 2017. EAF slag in asphalt mixes: A brief review of its possible re-use. *Resources, Conservation and Recycling*, 120, 176–185.
Sosa, I., et al., 2022. Durability of high-performance self-compacted concrete using electric arc furnace slag aggregate and cupola slag powder. *Cement and Concrete Composites*, 127, 104399.
Sun, Y.R., Wang, W.Y., and Chen, J.Y., 2019. Investigating impacts of warm-mix asphalt technologies and high reclaimed asphalt pavement binder content on rutting and fatigue performance of asphalt binder through MSCR and LAS tests. *Journal of Cleaner Production*, 219, 879–893.
Tang, X.W., et al., 2008. Study of 5.8 ghz magnetron in asphalt pavement maintenance. *Journal of Electromagnetic Waves and Applications*, 22 (14-15), 1975–1984.
Underwood, B.S., 2016. A continuum damage model for asphalt cement and asphalt mastic fatigue. *International Journal of Fatigue*, 82, 387–401.
Underwood, B.S., Kim, Y.R., and Guddati, M.N., 2006. Characterization and performance prediction of ALF mixtures using a viscoelastoplastic continuum damage model. *Asphalt Paving Technology*, 75, 577–636.
Underwood, B.S., Kim, Y.R., and Guddati, M.N., 2010. Improved calculation method of damage parameter in viscoelastic continuum damage model. *International Journal of Pavement Engineering*, 11 (6), 459–476.
Wang, C., et al., 2018. Laboratory investigation on chemical and rheological properties of bioasphalt binders incorporating waste cooking oil. *Construction and Building Materials*, 167, 348–358.
Wang, H., et al., 2019a. Laboratory and numerical investigation of microwave heating properties of asphalt mixture. *Materials*, 12, 146.
Wang, H., et al., 2020a. Accelerated healing in asphalt concrete via laboratory microwave heating. *Journal of Testing and Evaluation*, 48 (2), 739–757.
Wang, R., et al., 2020b. Investigating the effectiveness of carbon nanomaterials on asphalt binders from hot storage stability, thermodynamics, and mechanism perspectives. *Journal of Cleaner Production*, 276, 124180.
Wang, R., et al., 2021. Experimental study on mechanism, aging, rheology and fatigue performance of carbon nanomaterial/SBS-modified asphalt binders. *Construction and Building Materials*, 268, 121189.
Wang, R., et al., 2022. "Investigating the differences between steel slag and natural limestone in asphalt mixes in terms of microscopic mechanism, fatigue behavior and microwave-induced healing performance". *Construction and Building Materials*, 328, 127107.
Wang, Y., Liu, Z., and Hao, P., 2019b. Investigation on mechanical and microwave heating characteristics of asphalt mastic using activated carbon powder as electro-magnetic absorbing materials. *Construction and Building Materials*, 202, 692–703.
Wu, S., and Tahri, O., 2019. State-of-art carbon and graphene family nanomaterials for asphalt modification. *Road Materials and Pavement Design*, 22 (4), 735–756.
Yang, S., Mo, L., and Deng, M., 2021. Effects of ethylenediamine tetraacetic acid (EDTA) on the accelerated carbonation and properties of artificial steel slag aggregates. *Cement and Concrete Composites*, 118, 103948.
Yin, Y., et al., 2017. Effect of chemical composition of aggregate on interfacial adhesion property between aggregate and asphalt. *Construction and Building Materials*, 146, 231–237.
Zhai, Y., et al., 2018. Predicting the dielectric properties based on micromechanical modeling for asphalt mastics. *AIP Advances*, 8, 125311.
Zhang, M., et al., 2010. Magnetite/graphene composites: microwave irradiation synthesis and enhanced cycling and rate performances for lithium ion batteries. *Journal of Materials Chemistry*, 20 (26), 5538–5543.
Zhang, J., Sabouri, M., and Guddati, M.N., 2013. Development of a failure criterion for asphalt mixtures under fatigue loading. *Journal of Association of Asphalt Paving Technologists*, 82, 1–22.
Ziaee, S.A., and Behnia, K., 2020. Evaluating the effect of electric arc furnace steel slag on dynamic and static mechanical behavior of warm mix asphalt mixtures. *Journal of Cleaner Production*, 274, 123092.